



## Observation of two distinct, rapid loss mechanisms during the 20 November 2003 radiation belt dropout event

J. Bortnik,<sup>1</sup> R. M. Thorne,<sup>1</sup> T. P. O'Brien,<sup>2</sup> J. C. Green,<sup>3</sup> R. J. Strangeway,<sup>4</sup> Y. Y. Shprits,<sup>1</sup> and D. N. Baker<sup>5</sup>

Received 20 April 2006; revised 4 October 2006; accepted 18 October 2006; published 21 December 2006.

[1] The relativistic electron dropout event on 20 November 2003 is studied using data from a number of satellites including SAMPEX, HEO, ACE, POES, and FAST. The observations suggest that the dropout may have been caused by two separate mechanisms that operate at high and low  $L$ -shells, respectively, with a separation at  $L \sim 5$ . At high  $L$ -shells ( $L > 5$ ), the dropout is approximately independent of energy and consistent with losses to the magnetopause aided by the  $Dst$  effect and outward radial diffusion which can deplete relativistic electrons down to lower  $L$ -shells. At low  $L$ -shells ( $L < 5$ ), the dropout is strongly energy-dependent, with the higher-energy electrons being affected most. Moreover, large precipitation bands of both relativistic electrons and energetic protons are observed at low  $L$ -shells which are consistent with intense pitch angle scattering driven by electromagnetic ion cyclotron (EMIC) waves and may result in a rapid loss of relativistic electrons near the plasmapause in the dusk sector or in plumes of enhanced density.

**Citation:** Bortnik, J., R. M. Thorne, T. P. O'Brien, J. C. Green, R. J. Strangeway, Y. Y. Shprits, and D. N. Baker (2006), Observation of two distinct, rapid loss mechanisms during the 20 November 2003 radiation belt dropout event, *J. Geophys. Res.*, *111*, A12216, doi:10.1029/2006JA011802.

### 1. Introduction

[2] The trapped, energetic electron flux which makes up the Earth's radiation belts consists of an inner zone ( $L < 2$ ) which is relatively stable and an outer zone ( $L > 3$ ) which is highly dynamic and can vary by orders of magnitude over timescales ranging from minutes to decades [Blake *et al.*, 1992; Li *et al.*, 1993; Baker *et al.*, 1994; Selesnick and Blake, 1997; Onsager *et al.*, 2002]. Although the radiation belts have been studied for over 4 decades (e.g., see historical account by Stern [1996]), and the two-zone structure of the quiet time radiation belts has been explained in terms of inward radial diffusion and loss to the atmosphere [Lyons and Thorne, 1972], many of the processes responsible for the rapid variability of the outer belt are not fully understood [e.g., Friedel *et al.*, 2002; Reeves *et al.*, 2003; Green *et al.*, 2004].

[3] For instance, an examination of 276 moderate and intense geomagnetic storms from the period 1989–2000 [Reeves *et al.*, 2003] concluded that the radiation belt fluxes

behaved in an apparently unpredictable way and could increase, decrease, or remain relatively unchanged in response to the storm, independent of the strength of the storm or  $L$ -shell. This result suggested that the effect of geomagnetic storms on radiation belt fluxes is a delicate balance between the effects of particle acceleration and loss. In this paper we focus primarily on the rapid loss of radiation belt particles.

[4] Rapid losses of outer radiation belt electrons can be attributed to resonant wave-particle interactions between a variety of plasma waves and energetic electrons [e.g., Kennel and Engelmann, 1966], which drive pitch angle scattering into the drift and bounce loss cone.

[5] Quasi-linear estimates of the pitch angle scattering rates shows that whistler mode chorus waves could provide losses of the relativistic electrons on the timescale of a day [Albert, 2005; Horne *et al.*, 2005b; Thorne *et al.*, 2005]. The observed precipitation microbursts are thought to be related to the transient structure of the chorus waves [Lorentzen *et al.*, 2001]. EMIC waves preferentially generated in the high-density regions [Horne and Thorne, 1993] may provide even faster loss of MeV electrons on the scale of hours and affect only relativistic electrons since resonant energies for interactions with EMIC waves are above 0.5 MeV [Meredith *et al.*, 2003; Albert, 2003; Summers and Thorne, 2003]. Precipitation caused by EMIC waves may also be related to observations of hard X rays by balloon-borne instruments [Millan *et al.*, 2002].

[6] Losses to the magnetopause have been found to contribute to rapid outer radiation belt depletions [Desorgher *et al.*, 2000] and affect only those electrons that drift into the

<sup>1</sup>Department of Atmospheric and Oceanic Sciences, University of California, Los Angeles, California, USA.

<sup>2</sup>Space Sciences Department/Chantilly, The Aerospace Corporation, Chantilly, Virginia, USA.

<sup>3</sup>NOAA, Boulder, Colorado, USA.

<sup>4</sup>Institute of Geophysics and Planetary Physics, University of California, Los Angeles, California, USA.

<sup>5</sup>Laboratory for Atmospheric and Space Physics, University of Colorado, Boulder, Colorado, USA.

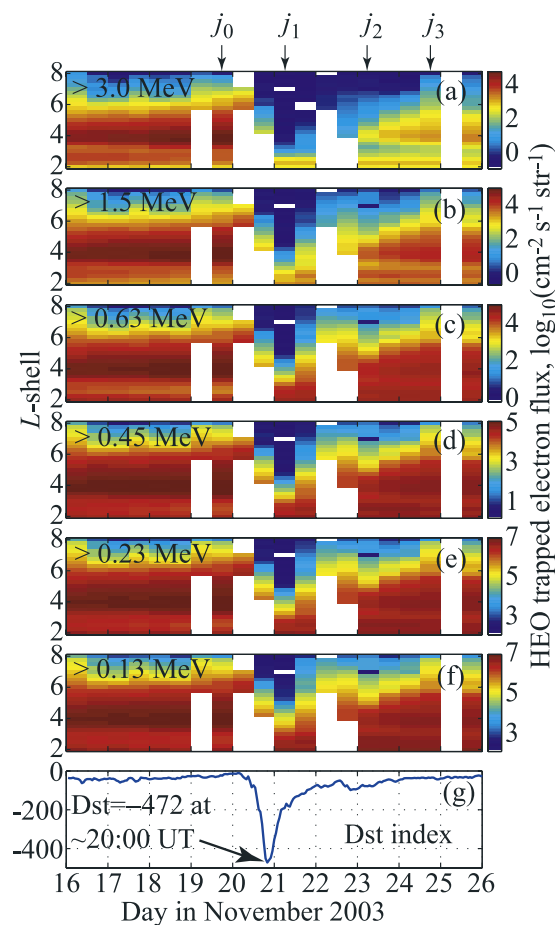


**Figure 1.** HEO fluxes shown as a function of  $L$ -shell and time for (a)  $E > 3$ , (b)  $E > 1.5$ , (c)  $E > 0.63$ , (d)  $E > 0.45$ , (e)  $E > 0.23$ , and (f)  $E > 0.13$  MeV and (g)  $Dst$  for this period.

magnetopause [Green *et al.*, 2004]. However the inward radial gradients, created by these losses may drive outward radial diffusion and produce losses of relativistic electrons down to the heart of the radiation belts [Shprits *et al.*, 2006b] and significantly deplete outer radiation belt fluxes during the main phase of the storm on the timescale of hours. For equatorially mirroring particles, electrons could also be significantly transported to the magnetopause by the  $Dst$  effect.

[7] Fast nonadiabatic losses are often observed during the main phase of storms [Nagai, 1988, Mathie and Mann, 2000; Desorgher *et al.*, 2000; Onsager *et al.*, 2002; Green *et al.*, 2004]. An example of a rapid electron flux loss (or “dropout”) event in the outer belt has recently been reported by Onsager *et al.* [2002], where the  $>2$  MeV electron flux decreased by  $\sim 3$  orders of magnitude in a period of several hours. In a subsequent study, Green *et al.* [2004] used 52 similar dropout events to perform a superposed epoch analysis and test a number of loss mechanisms that may contribute to the flux decreases, including adiabatic electron motion (in response to a buildup of the ring current and lowered magnetic field intensities), magnetopause encounters, and precipitation to the atmosphere. The study con-

cluded that precipitation to the atmosphere was most likely the cause of the dropout, but the cause of the precipitation was uncertain [Green *et al.*, 2004].

[8] In the current paper the dropout event that occurred on 20 November 2003 is analyzed. This period was chosen because (1) of the intensity of the event, the provisional  $Dst$  index reached  $-472$  nT making it the second largest storm in the interval 1957–2004 [Ebihara *et al.*, 2005], (2) the extensive satellite coverage and high quality of data available in this period, and (3) the attention that this interval received in the literature [e.g., Ebihara *et al.*, 2005; Foster *et al.*, 2005; Meier *et al.*, 2005; Yizengaw *et al.*, 2006], which facilitates discussion and comparison to related observations. In section 2, data is presented from a number of satellites showing the evolution of the dropout event, and section 3 gives a discussion of the observations, an interpretation of the physical process involved, and relation of these results to similar studies.

## 2. Observations

[9] Observations from a number of satellites are used to analyze the 20 November 2003 dropout event. These satellites include:

[10] 1. The Highly Elliptical Orbiter HEO-3 (1997-068) satellite, altitude  $\sim 1.1 \times 7$  Re, inclination  $\sim 62^\circ$ , period  $\sim 12$  hours (see Blake *et al.* [1997] for HEO orbit), to measure trapped electron fluxes as a function of energy.

[11] 2. The Solar, Anomalous, and Magnetospheric Particle Explorer (SAMPEX) satellite, altitude  $\sim 600$  km, inclination  $\sim 82^\circ$ , orbit  $\sim 100$  min [Baker *et al.*, 1993], to measure precipitating relativistic electron fluxes ( $>1$  MeV) and trapped/quasi-trapped electron fluxes (2–6 MeV).

[12] 3. The Advanced Composition Explorer (ACE) satellite, orbiting around the Sun-Earth L1 libration point at 240 Earth radii sunward of the Earth [Stone *et al.*, 1998], used to measure solar wind parameters to calculate the location of the magnetopause.

[13] 4. The Polar-orbiting Operational Environmental Satellite (POES), altitude  $\sim 833$  km, inclination  $98.6^\circ$  [Evans and Greer, 2000], to measure precipitating proton fluxes.

[14] 5. The Fast Auroral Snapshot (FAST) mission, altitude  $350 \text{ km} \times 4175 \text{ km}$ , inclination  $83^\circ$ , period  $\sim 130$  min [Carlson *et al.*, 1998], to measure electron and proton fluxes and pitch angle distributions near the auroral oval boundary.

[15] The observations from all the above satellites are presented in this section, with specific instrument descriptions attached to the relevant observations. The discussion and interpretation are given in the following section.

[16] In Figures 1a–1f, the omnidirectional integrated energetic electron fluxes from HEO-3, which reflect primarily trapped electron fluxes, are shown as a function of  $L$ -shell and time, above various energy thresholds for a 10-day interval surrounding the dropout event. From top to bottom, the energy thresholds are 3, 1.5, 0.63, 0.45, 0.23, and 0.13 MeV. The provisional  $Dst$  index is shown in Figure 1g, obtained from the World Data Center, Kyoto, Japan. The white areas in the figures correspond to periods where no data was available.

[17] In the periods surrounding the dropout event (before 20 November and after 22 November), the radiation belt fluxes increase due to acceleration processes that occur on

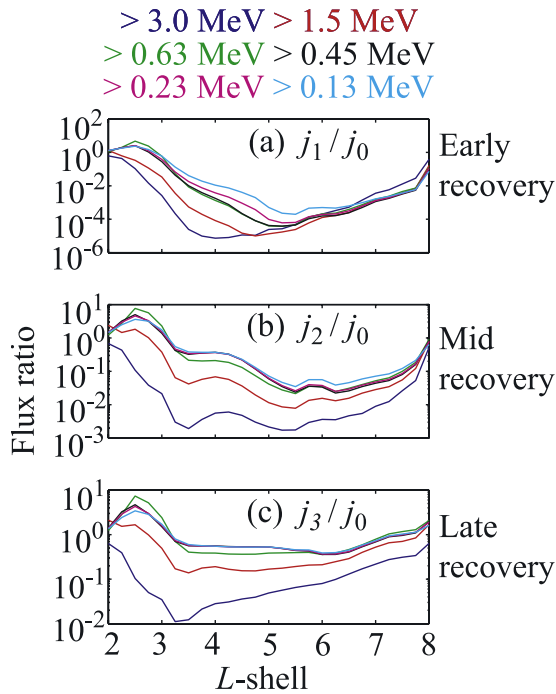


**Figure 2.** Ratio of fluxes in the (a) early, (b) middle, and (c) late recovery periods to the flux before the storm main phase, shown in Figure 1.

timescales of days [e.g., *Horne et al.*, 2005a, 2005b; *Shprits et al.*, 2006a], but during the dropout event itself the fluxes decrease beginning at the higher  $L$ -shells early on 20 November and progress as a function of time to lower  $L$ -shells, where they reach a minimum early on 21 November. It is not clear what happens at the lower  $L$ -shells during this interval since data is missing. However, it is apparent that the loss of electrons is more dramatic at higher energies at all  $L$ -shells, whereas the low energies exhibit dramatic losses only at the higher  $L$ -shells, suggesting that different processes might be operating at higher  $L$ -shells ( $L > 5$ ) compared to lower  $L$ -shells ( $L < 5$ ).

[18] To emphasize the difference in response between the higher ( $E \geq 0.63$  MeV) and lower ( $E \leq 0.45$  MeV) energy channels, we compared the flux in three time intervals after the dropout, marked  $j_1$ ,  $j_2$ , and  $j_3$  in Figure 1, with the flux before the dropout, marked  $j_0$ . Flux ratios as a function of  $L$ -shell, parametrized and color-coded by energy channel are shown in Figure 2. During the storm main phase and early recovery (Figure 2a), it is evident that at low  $L$ -shells the dropout is clearly energy-dependent with the higher energies exhibiting the most dramatic depletion, whereas at  $L > 5$  the dropout is approximately the same for all energies. There is thus an apparent separation at  $L \sim 5$  indicating that there may be different mechanisms acting to deplete the lower  $L$  region and higher  $L$  regions respectively.

[19] It should also be noted that in the late recovery period (Figure 2c), when  $Dst$  returns to its prestorm value, low  $L$ -shell fluxes at the lower energies ( $E \leq 0.45$  MeV) return to their prestorm values, indicating that the depletion may have been caused by the  $Dst$  effect and not by a real loss, whereas fluxes at the higher energies ( $E \geq 0.63$  MeV) do not return to

their prestorm values, indicating that there is a real loss of particles from the system. Consistent with Figure 2a, the nonadiabatic particle loss increases with increasing energy, and extends to low  $L$ -shell. The interpretation of the dropout event from the late-recovery flux measurements (Figure 2c) is complicated by the fact that a number of additional processes have come into play at this time, such as local acceleration, strong radial diffusion driven by ULF waves, and convection of lower energy electrons. Consequently, any further conclusions about Figure 2c should be made with caution.

[20] During the trapped flux dropouts, which are observed by HEO, the Heavy Ion Large Telescope (HILT) instrument on SAMPEX shows evidence of intense electron precipitation bands (PBs) [*Nakamura et al.*, 1995], which are shown in Figure 3 (black line plot) as localized flux enhancements above the SAMPEX drift loss cone background. Because of its wide angular acceptance of  $68^\circ \times 68^\circ$  [*Blake et al.*, 1996], HILT monitors both the drift loss cone flux, which is strongly dependent on geographical location, and the bounce loss cone flux, showing more localized enhanced precipitation. As an estimate of the background drift loss cone flux, Figure 3 (grey) shows line plots of the fluxes observed by HILT on 19 November 2003 (quiet day preceding the storm) for SAMPEX orbits which are as similar to the storm-day orbits as possible. A summary of the key parameters taken at the center of the respective SAMPEX passes is given in Table 1, where each of the four rows corresponds to a panel in Figure 3, and the upper and lower lines within each row correspond to the black and gray line plots, respectively, showing the similarity in the chosen orbits.

[21] The PBs shown in Figure 3 are identified as flux enhancements which clearly stand out above the background (a factor greater than  $\sim 3$  above the ambient flux levels), and

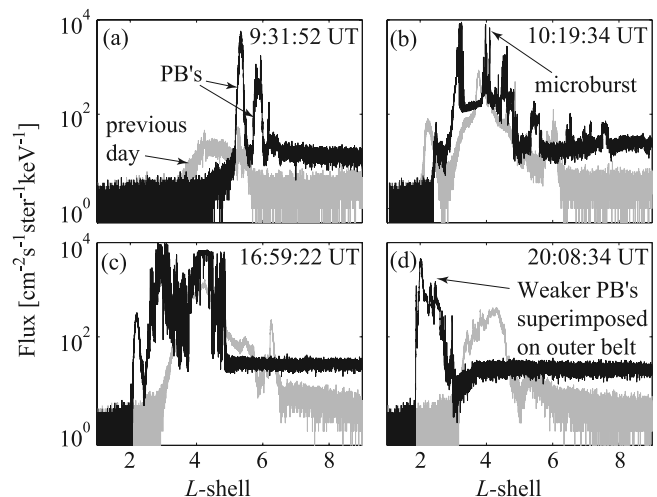


**Figure 3.** SAMPEX data showing examples of precipitation bands on 20 November 2003, at (a) the beginning of the storm and (b,c) during the main phase. (d) After  $\sim 2000$  UT, there is evidence of weaker precipitation superposed on the remnants of the outer belt, which has now moved to low  $L$ -shells. In gray we show the SAMPEX flux at approximately the same location, on the previous day (19 November 2003), for comparison.

**Table 1.** Key Parameters (Date, Time, Magnetic Local Time, Geographic Latitude and Longitude) Describing the Storm Time (11/20/2003) and Reference (11/19/2003) SAMPEX Flux Observations Shown in Figure 3<sup>a</sup>

Row	Date	Time, UT	MLT	Geographic Latitude	Geographic Longitude
A1	11/20/2003	0931:52	13.6	41.1°	56°
A2	11/19/2003	0954:27	13.8	41.3°	52.4°
B1	11/20/2003	1019:34	2.7	-39°	224.5°
B2	11/19/2003	1042:15	2.8	-38.7°	221°
C1	11/20/2003	1659:22	2.4	42.1°	138.5°
C2	11/19/2003	1722:03	2.6	42.4°	134.9°
D1	11/20/2003	2008:34	2.2	42.9°	91.1°
D2	11/19/2003	2031:03	2.3	42.4°	87.4°

<sup>a</sup>The given values are recorded at the center of the SAMPEX pass, the four rows (A–D) correspond to Figures 3a–3d, and within each row the upper values (1) correspond to the storm-time fluxes, and lower line (2) corresponds to the reference fluxes (black and gray line-plots in Figure 3, respectively).

have a spatial extent comparable to a few tenths of an  $L$ -shell. This definition of a PB is consistent with earlier observations [Nakamura *et al.*, 1995] which reported a typical duration of  $\sim 10$ – $30$  s for each precipitation band when observed along a SAMPEX satellite track. For reference, the SAMPEX satellite travels roughly 80 km in 10 s (corresponding to  $0.13L$  near  $L = 4$ ), making the spatial extent of a PB consistent with our definition.

[22] The spatially extended PBs shown in Figure 3 are distinct from previously reported electron microbursts in a few respects: microbursts are typically of short duration, lasting a few tenths of a second, occur preferentially in the dawn sector, are confined to regions of low plasma density, e.g., outside the plasmapause, and show a strong association with whistler-mode chorus [Blake *et al.*, 1996; Lorentzen *et al.*, 2001; O'Brien *et al.*, 2004; Thorne *et al.*, 2005]. In contrast, statistical information on the distribution of PBs

[Nakamura *et al.*, 1995, 2000; O'Brien *et al.*, 2005] indicates that they are long lasting (10–30 s as described above) and occur typically in the premidnight sector, in the range  $L = 4$  to 6, but a particular causative mechanism has not yet been firmly established. A possible mechanism is scattering by electromagnetic ion cyclotron waves (EMIC) waves, which we discuss further in section 3. Another possibility is scattering by electrostatic ion cyclotron waves [e.g., Koons *et al.*, 1972; Vampola, 1977], but the  $L$  values seen here appear to be too low for such waves, which are usually associated with auroral field-aligned currents, as we discuss further below. Also evident in Figure 3 is the motion (as a function of time) of the PBs to lower  $L$ -shells and their simultaneous intensification. The radial position and intensity of the PB's observed on 20–22 November are shown as a function of time and  $L$ -shell in Figure 4 as the colored vertical lines. The color scale on the right of the figure represents the intensity of each

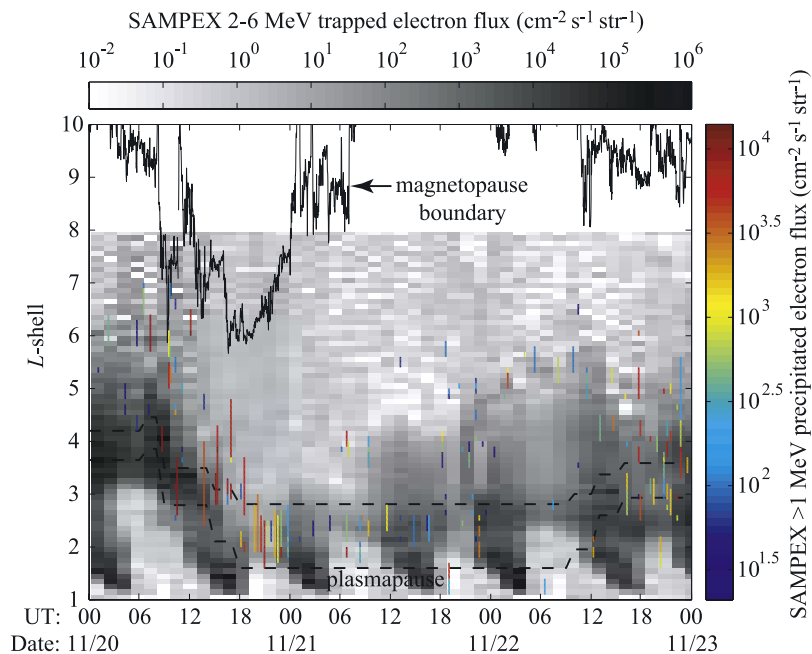


**Figure 4.** Composite plot showing magnetopause standoff distance from Shue *et al.* [1998] (solid line), minimum and maximum locations of plasmapause from O'Brien and Moldwin [2003] (dashed lines), SAMPEX 2–6 MeV trapped fluxes in grayscale, and superposed SAMPEX precipitation bands (vertical colored lines).

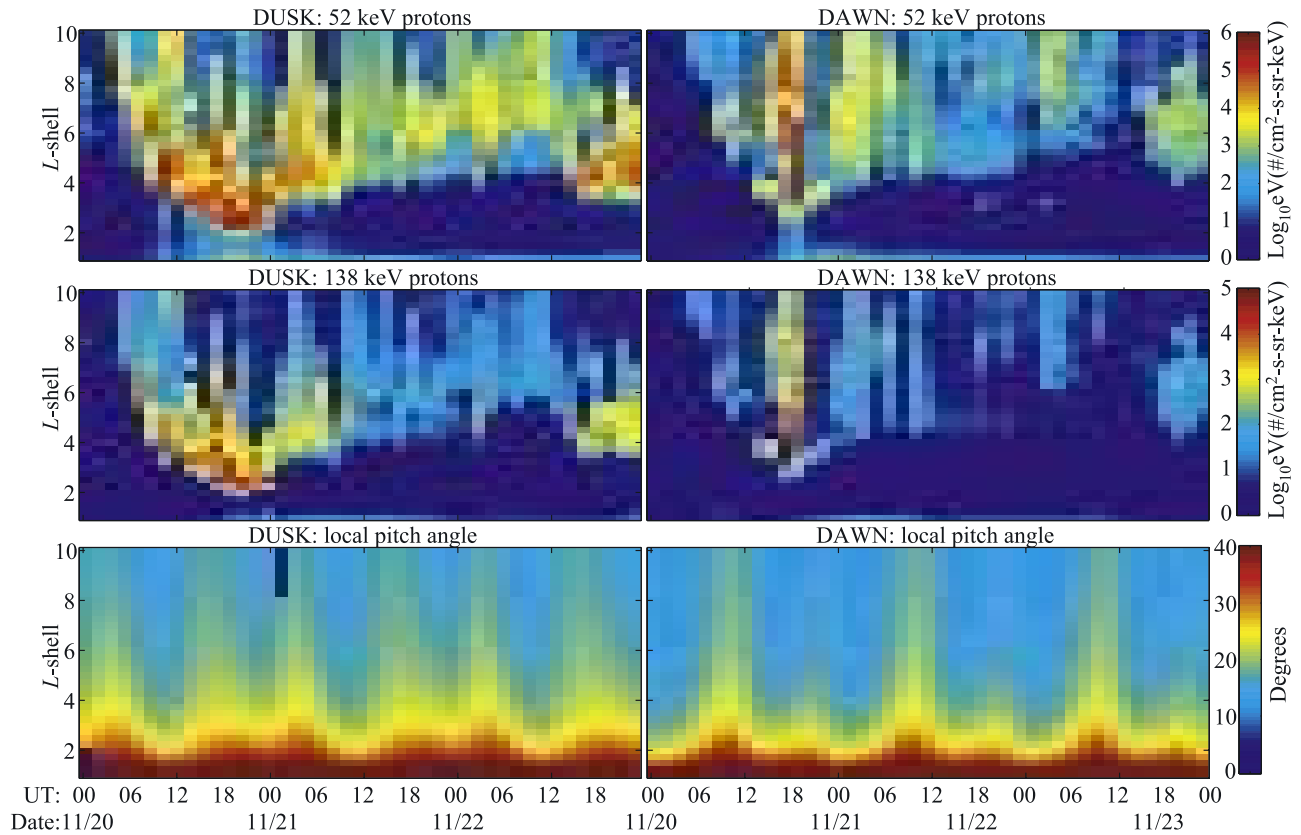


**Figure 5.** POES satellite data showing northern hemisphere precipitating proton fluxes as a function of  $L$ -shell and time, for dusk (left column) and dawn (right column) sectors, and low (52 keV) and high (138 keV) energy channels in the upper and lower rows, respectively. The detector pointing angle is given in the bottom panels.

PB. Trapped electron flux measured using the ELO channel (2–6 MeV) of the PET instrument aboard SAMPEX [Cook *et al.*, 1993] is superimposed in grayscale for comparison. Diurnal variations in PET flux are due to the geocentric offset of the Earth’s nominally dipolar magnetic field and resultant asymmetric features, e.g., the South Atlantic Anomaly.

[23] The estimated minimum and maximum locations of the inner edge of the plasmopause [O’Brien and Moldwin, 2003], calculated using the Kp index as the input, are overlaid as dashed lines on Figure 4. During the main phase of the storm, the most intense PBs appear to track the inward motion of the plasmopause whereas under quiet conditions PB are found at higher  $L$ , close to the outer edge of the trapped flux. The estimated position of the magnetopause is also shown as a solid line, calculated using the Shue *et al.* [1998] model, with inputs from the ACE satellite [Stone *et al.*, 1998], propagated to  $\sim 15$  Re [Weimer *et al.*, 2003]. The magnetopause is clearly very compressed during the interval of the dropout, reaching  $L \sim 6$  at  $\sim 1000$  UT and again at  $\sim 1600$  UT. The magnetopause acts as an absorbing boundary condition to radiation belt electrons, since electrons that drift beyond this boundary are rapidly demagnetized, and permanently lost (magnetopause shadowing) [e.g., West *et al.*, 1972]. As the magnetopause moves closer to the Earth, there may also be loss from  $L$ -shells lower than the magnetopause

boundary due to drift (caused by the  $Dst$  effect, during the buildup of the ring current in the main phase of the storm) or diffusion (due to inward radial gradients in the phase space density) [Shprits *et al.*, 2006b].

[24] Intense proton precipitation structures (Figure 5) were observed on the NOAA POES satellite using the Medium Energy Proton and Electron Detector (MEPED) [Evans and Greer, 2000]. The MEPED instrument has a full-cone angle of  $30^\circ$ , and the pointing direction relative to the magnetic field is shown in the bottom panels of Figure 5 for the dusk and dawn passes, respectively.

[25] These proton precipitation structures are coincident in time and  $L$ -shell with those observed on SAMPEX and henceforth referred to as proton PBs because of their similarity in  $L$  structure to the electron PBs observed on SAMPEX (Figure 4). The left and right columns of Figure 5 correspond to northern hemisphere dusk and dawn passes, respectively, and the top and bottom rows correspond to the low ( $\sim 52$  keV) and high ( $\sim 138$  keV) energy channels, respectively, determined from the bowtie method described by Selesnick and Blake [2000]. As shown, both energy channels behave in a similar way and show intense proton PBs that intensify as a function of time on 20 November, while simultaneously moving to lower  $L$ -shells. The peak in intensity occurs near 0000 UT on 21 November, and then weakens by a factor of 10–100 later on 21 November. The

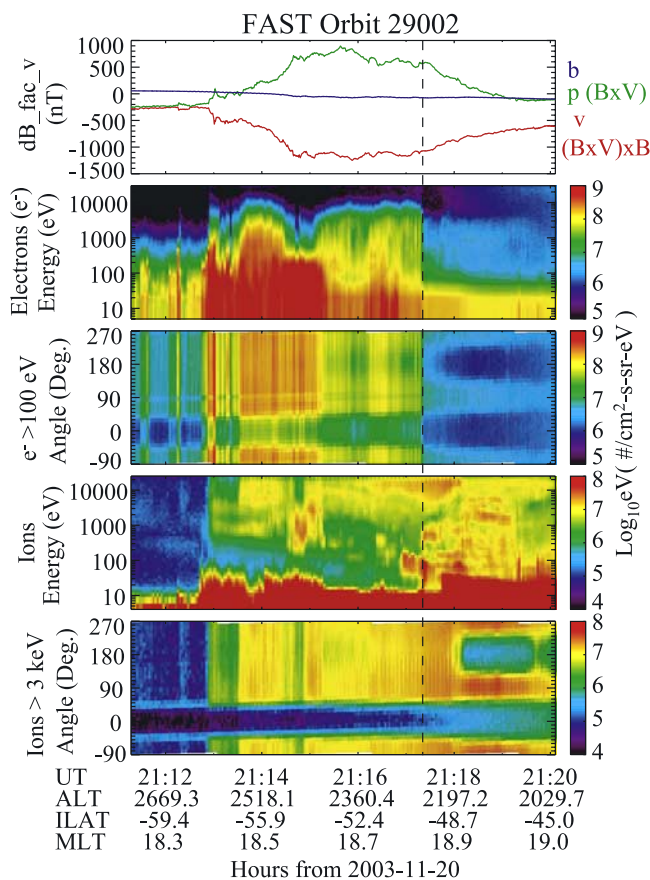


**Figure 6.** Data acquired by the FAST spacecraft in the dusk local time sector on orbit 29002, 20 November 2003. The data were acquired in the southern hemisphere where the ambient magnetic field points away from the Earth. Precipitating particles therefore have  $180^\circ$  pitch angles. The vertical dashed line at 21:17:20 UT indicates the equatorward boundary of the auroral region.

behavior of the PBs on the dawn and dusk shows strong asymmetry, the precipitation on the dusk being a few orders of magnitude more intense than that on the dawnside, indicating that the majority of the pitch angle scattering occurs on the duskside consistent with scattering by EMIC waves as discussed in section 3. The low energy precipitating electron data is not shown because it is believed to be contaminated at this time.

[26] It is interesting to locate the PBs in relation to the auroral oval boundary during the dropout period, and for this purpose a typical observation from the FAST satellite [Carlson *et al.* 1998] is shown in Figure 6. The electrostatic analyzers and magnetometer that acquired these are described by Carlson *et al.* [2001] and Elphic *et al.* [2001], respectively. The figure shows from top to bottom magnetic field perturbations cast into a field-aligned coordinate system (Figure 6a); electron flux averaged over all pitch angles as a function of energy and time for energies  $< 30$  keV (Figure 6b); electron flux in the range  $100 \text{ eV} < E < 30 \text{ keV}$  as a function of pitch angle and time (Figure 6c); ion flux averaged over all pitch angles (Figure 6d); and ion flux in the range  $3 \text{ keV} < E <$

$30 \text{ keV}$  as a function of pitch angle and time (Figure 6e). The magnetic field perturbations are shown in a direction nominally along the spacecraft velocity vector (red), across the spacecraft track (green) and along the ambient magnetic field (blue). Since the data in Figure 6 were acquired in the southern hemisphere, a negative (positive) gradient in the green trace corresponds to an earthward (antearthward) field-aligned current. The large fluxes of electrons between 2113 and 2115 UT in Figure 6 are presumably the current carriers for the antearthward current, indicated by the positive slope in the green trace. For the southern hemisphere it is worth remembering that  $180^\circ$  pitch angle corresponds to precipitating particles; the loss cone in the southern hemisphere is at  $0^\circ$  pitch angle.

[27] At 21:17:20 UT (dashed line Figure 6), the flux of precipitating electrons suddenly decreases, indicating a transition out of the auroral region. On the other hand, the flux of precipitating ions above 3 keV (with essentially gyrotropic distributions over the downward loss cone) intensifies outside the auroral region, and is observed for another 40 s indicating the presence of a scattering mechanism. The  $> 3 \text{ keV}$  ions display a double loss cone after 21:18:00 UT (below  $L \sim 2.3$ ). The fact that large fluxes of precipitating ions are observed at lower latitudes than the auroral region (marked by precipitating electrons) suggests that strong pitch angle scattering at the equator is responsible for the filled loss cone, rather than local scattering through waves generated by auroral electrons. The  $L$  region of precipitating ions observed on FAST is also consistent with the location of the ion PBs observed on POES (and electron PBs observed on SAMPEX) and similarly occurs primarily on the duskside. It is noted that there is an absence of precipitating, low-energy ( $< 30 \text{ keV}$ ) electrons from Figure 6b, consistent with scattering by EMIC waves, which have a minimum resonant energy of  $\sim 0.5 \text{ MeV}$ . Thus a prime candidate for the strong precipitation is scattering by EMIC waves, as discussed in the next section.

### 3. Discussion

[28] Using the available data presented in Figures 1–6, we suggest that the dropout event on 20 November 2003 was caused by two different loss mechanisms acting at high and low  $L$  regions, respectively.

[29] At high  $L$ -shells, the magnetopause becomes compressed to  $L \sim 6$  briefly at  $\sim 1000$  UT on 20 November and for a more extended period at  $\sim 1600$  UT on 21 November, which causes energetic electrons to be lost directly to this boundary within one drift period [West *et al.*, 1972]. However, magnetopause shadowing can remove energetic electrons from regions much deeper within the magnetosphere through the so-called “Dst effect” [Dessler and Karplus, 1961; Kim and Chan, 1997], which is simply a result of the buildup of the ring current, a consequent reduction of the strength of the main field of the Earth, and conservation of all three adiabatic invariants of the particles. For example, Kim and Chan [1997] estimate that when  $Dst = -100 \text{ nT}$ , the particles observed at Geosynchronous Earth Orbit ( $L = 6.6$ ) have been transported there from regions near  $L \sim 5-5.5$ , depending on which magnetic field model is used (i.e., a change in location of 1–1.5  $L$ -shells). In our case,  $Dst = -472 \text{ nT}$  and the change in  $L$ -shell is expected to be much

larger, but to be conservative we will assume it is  $\sim 1$   $L$ -shell (due to other factors such as field line compression on the day side [e.g., Roederer, 1970] and inaccuracies in modeling the ring current in this period), potentially bringing particles to the magnetopause boundary ( $L \sim 6$ ) from as low as  $L \sim 5$  or lower. Accurate assessment of the full effect of magnetopause shadowing combined with the *Dst* effect is a complex problem, which is well beyond the scope of the current paper. On the other hand, outward radial diffusion may be the dominant mechanism in removing energetic electrons from high  $L$ -shells due to the large negative radial gradients that develop in phase space, and rapid increase of the radial diffusion coefficient with  $L$ -shell [Brautigam and Albert, 2000]. Quantitative assessment of outward radial diffusion during the 20 November 2003 dropout event has indicated that this mechanism can deplete energetic electrons to  $L \sim 4$ – $5$  over appropriate timescales consistent with observations [Shprits et al., 2006b].

[30] Figure 2a indicates that below  $L \sim 5$ , the depletion of flux is dramatically different between high- and low-energy channels. The high energies ( $E > 3$  MeV,  $E > 1.5$  MeV) are severely depleted (factor of  $\sim 10^{-5}$ ), with the region of maximum depletion moving to lower  $L$ -shells with increasing energy. The low energy channels ( $E > 0.13$  MeV,  $E > 0.23$  MeV,  $E > 0.45$  MeV,  $E > 0.65$  MeV) on the other hand, show a far weaker depletion (factor of  $\sim 10^{-2}$ ) which is independent of energy below  $L \sim 3.5$ . Between  $L \sim 3.5$  and  $5$ , the relative change of flux is energy-dependent for all channels, with the higher energies being affected most.

[31] The region where the higher energy fluxes are depleted most severely ( $L \sim 3$ – $4$ ) coincides with the region in Figures 4 and 5 where the most intense and spatially extended PBs are observed. As mentioned above, the PBs also track the location of the plasmopause. Finally, we note that the observation of the PBs in the SAMPEX orbit ( $\sim 2$ – $1400$  MLT meridian) was not symmetrical. Most PB observations occurred on the nightside, implying that the scattering into the drift and bounce loss cones must have occurred at locations west of the observation, i.e., in the dusk sector. During the entire 3-day period of 20–22 November, 65% of PB observations occurred on the nightside, but in the most intense precipitation interval, 20 November, 1200–2000 UT (see Figure 4), 100% of PB observations occurred on the nightside. The fact that scattering was highly asymmetric and far more intense on the duskside is confirmed by precipitating proton measurements shown in Figure 5.

[32] The characteristics of PBs reported above are consistent with pitch angle scattering by electromagnetic ion cyclotron (EMIC) waves [Thorne and Kennel, 1971; Lyons and Thorne, 1972]. Such waves occur preferentially near the dusk sector, are very intense (1–10 nT) [Erlanson and Ukhorskiy, 2001; Fraser and Nguyen, 2001], and can drive strong pitch angle diffusion [Albert, 2003; Summers and Thorne, 2003] of relativistic electrons and energetic protons. Furthermore, EMIC waves resonate only with high-energy electrons (consistent with the energy-dependent loss shown in Figure 2), which have minimum values as low as  $E \sim 0.5$  MeV in high density plumes or at the plasmopause [Meredith et al., 2003], where the ring current overlaps the plasmopause causing EMIC excitation [Cornwall et al., 1970]. Observations on the FAST satellite (Figure 6, second

panel) of low-energy ( $< 30$  keV) precipitating electrons confirm that there is no component of low-energy precipitating electrons coincident with the SAMPEX PBs observations, consistent with scattering by EMIC waves.

[33] Ion scattering by EMIC waves (as shown in Figure 5) is expected theoretically and commonly observed during storm times [Jordanova et al., 2003; Walt and Voss, 2004]. On 20 November, strong ion precipitation was observed by the FAST and POES satellites coincident with the PBs observed on SAMPEX, which occurred preferentially on the dusk side as expected from scattering by EMIC waves near the plasmopause and plasmaspheric drainage plumes [e.g., Spasojevic et al., 2005]. The ionospheric footprint of a very dense plume was indeed observed at the beginning of this event using multiple instruments on the ground [Foster et al., 2005].

[34] Ring current simulations and observations of the present event [Ebihara et al., 2005] show that the ring current moved inward to extremely low  $L$ -shells ( $L \sim 1.5$ ), providing a free energy source for EMIC excitation [Jordanova et al., 2003]. However, the charge exchange process by itself could not account for the rapid decay of the ring current at low  $L$ -shells, even when very high concentrations of hydrogen were used. Ebihara et al. [2005] used an ad hoc pitch angle diffusion coefficient to simulate loss of ring current particles which gave the appropriate decay. This gives further support to the hypothesis that intense EMIC waves were present during the 20 November dropout event at low  $L$ -shells, and were responsible for the scattering of both ring current protons and relativistic electrons [e.g., Thorne et al., 2006]. Further evidence of the presence of EMIC waves (and associated thermal electron heating [Cornwall et al., 1970]) at low latitudes is found indirectly through studies of thermosphere heating in this period, where a “tongue” of increased temperature (possibly related to a plasmaspheric plume) is observed [Meier et al., 2005]. Previous studies which have examined a large number of dropout events also concluded that enhanced precipitation into the atmosphere is likely to cause the rapid loss but did not identify a mechanism [Green et al., 2004].

[35] While the focus of the observations in Figures 1–6 has been on the precipitating electrons, i.e., low pitch angle ( $\alpha \sim 0^\circ$ ) particles, mention should be made of the scattering mechanisms believed to be responsible for the diffusion of particles at higher pitch angles ( $\alpha \sim 90^\circ$ ) too, since the dropout shown in Figure 1 occurs over all  $\alpha$ . Using quasilinear diffusion theory, the scattering of  $\sim 1$  MeV electrons by EMIC waves was shown to be most effective from the loss cone to  $\alpha \sim 60^\circ$  [Albert, 2003; Glauert and Horne, 2005]. At higher pitch angles, EMIC waves alone are insufficient to cause rapid diffusion and other wave modes are required, which are most likely chorus and/or hiss. Chorus waves have been shown to significantly intensify with magnetic activity [Meredith et al., 2001] and cause pitch angle scattering which is peaked at  $\alpha \sim 50^\circ$ – $90^\circ$  for  $\sim 1$  MeV electrons [Horne et al., 2005a, 2005b]. Hiss similarly tends to intensify with increasing geomagnetic activity, and affects particles of medium to high pitch angles. Although the intensity of hiss is significantly weaker than that of EMIC waves, the MLT region occupied by hiss is larger and in fact when spatial distribution is taken into account, it can be shown that under a certain set of assumption the overall pitch angle scattering by hiss at

medium to high pitch angles ( $\alpha \sim 30^\circ - 90^\circ$ ) is comparable to that by EMIC at low pitch angles [Albert, 2003]. On the other hand, scattering by electrostatic waves associated with auroral field-aligned currents is considered less likely because such waves typically occur within a few thousand kilometers of the auroral ionosphere [Cattell *et al.*, 2002] where wave-particle interactions are relatively inefficient due to the large inhomogeneity in B-field. Furthermore, the range of pitch angles affected is very small, for example the equatorial pitch angle ( $\alpha_{eq}$ ) for an electron mirroring at 100 km and 3000 km at  $L = 3$  is  $\alpha_{eq}(100 \text{ km}) = 8.6^\circ$  and  $\alpha_{eq}(3000 \text{ km}) = 15.8^\circ$ , respectively, giving an affected range of only  $\sim 7.2^\circ$ . At  $L = 5$ , the equatorial pitch angles become  $\alpha_{eq}(100 \text{ km}) = 3.9^\circ$  and  $\alpha_{eq}(3000 \text{ km}) = 6.9^\circ$ , giving a range of  $\sim 3^\circ$  which again underscores that fact that such waves are not dominant in emptying out the radiation belts over short timescales. The fact that the auroral region does not overlap with the region of intense proton precipitation has been shown with a typical FAST observation in Figure 6 and further supports our conclusion. The final point which must be noted about scattering at high pitch angles is that electron lifetimes are most sensitive to the value of the pitch angle diffusion coefficient near the loss cone, and as long as moderate pitch angle diffusion exists at higher pitch angles, the gradient in phase space as a function of pitch angle ( $\partial f / \partial \alpha$ ) will adjust to compensate for any changes in the pitch angle diffusion coefficient ( $D_{\alpha\alpha}$ ) so that the product of the two,  $(\partial f / \partial \alpha)(D_{\alpha\alpha})$ , will remain approximately constant after a few drift periods. Sensitivity experiments show that even when  $D_{\alpha\alpha}$  is decreased by an order of magnitude over a  $15^\circ$  pitch angle range at a location away from the loss cone, the effective electron lifetime is decreased by a factor less than two [Shprits *et al.*, 2006c].

[36] Our proposed sequence of events is summarized in Figure 7, where we show the instantaneous position of magnetopause boundary calculated using the empirical model of Shue *et al.* [1998], average plasmapause location [O'Brien and Moldwin, 2003], location of precipitation bands from SAMPEX occurring within 30 min of the displayed time stamp of each figure, and an expected plume location which we have simply drawn in, in approximate agreement with the ionospheric "tongue of ionization" given by Foster *et al.* [2005] at this time (IMAGE data for this period was not available). After the initial quiet period (Figure 7a), a strong convective E-field drives plasma sheet protons toward the Earth, which then experience a gradient-curvature drift westwards in the Earth's magnetic field. When the protons drift into regions of higher electron density, such as the plasmapause or plasmaspheric drainage plumes, they become highly unstable to EMIC wave growth, resulting in EMIC waves that scatter relativistic electrons (Figure 7b) and protons into the bounce and drift loss cones [e.g., Jordanova *et al.*, 2003; Lorentzen *et al.*, 2000]. The electrons in the drift loss cone then continue drifting eastwards, where they are observed by SAMPEX (as we have demonstrated in this paper) and are lost in the South Atlantic Anomaly within one drift period. Higher pitch angle electrons drift through the dawnside where intense chorus scatters their pitch angles to lower values, and when these particles enter higher-density regions (also where the EMIC waves are located) intensified hiss scatters the high and medium pitch angle particles to still lower values (Figure 7e). Simultaneously, the compres-

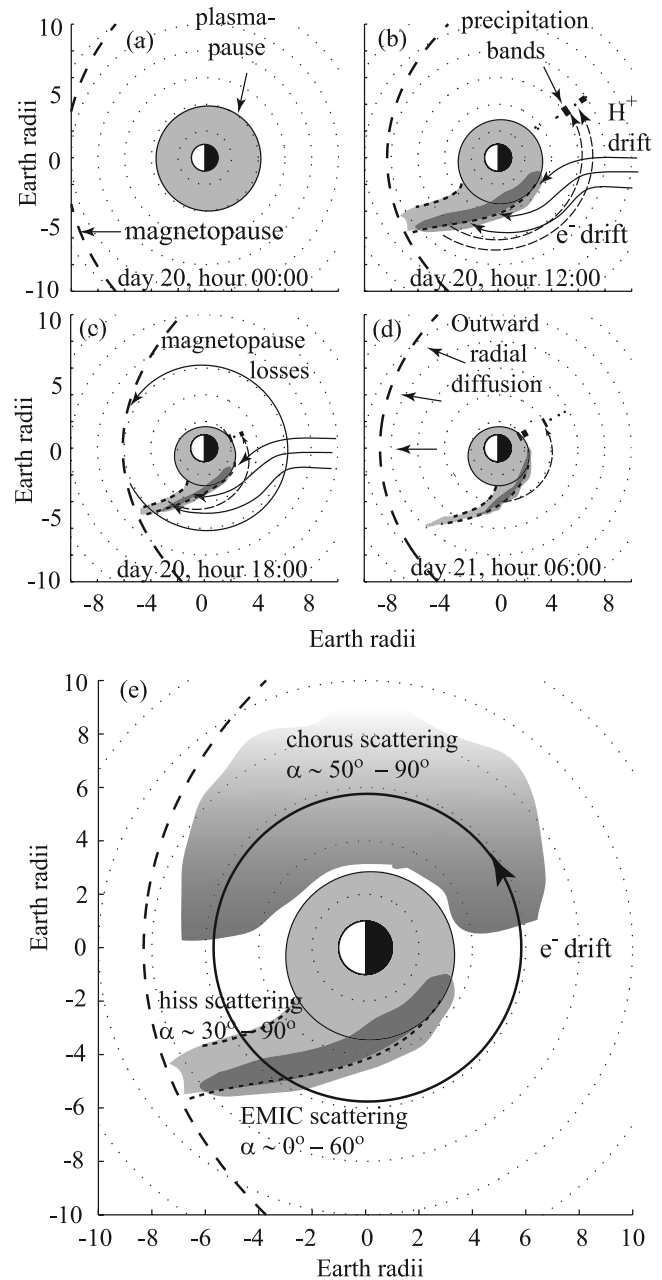


**Figure 7.** Illustration of the sequence of events: (a) Prestorm (quiet) conditions, (b) inward convection of plasma sheet ions, growth of EMIC waves at the plasmapause and plume, and subsequent observation of PBs depleting the lower  $L$  region, (c) rapid magnetopause losses reducing the flux at the outer boundary, coupled with the  $Dst$  effect, (d) outward radial diffusion depleting the higher  $L$  region, and (e) trajectory of high pitch angle particles and pitch angle scattering by storm-enhanced chorus, hiss, and EMIC waves. Dotted circles represent lines of constant radius in all plots.

sion of the magnetopause, coupled with the  $Dst$  effect and enhanced radial diffusion, brings particles from  $L$ -shells as low as  $L \sim 5$  to the magnetopause, where they are permanently lost (Figure 7c). Finally, the magnetopause relaxes and ring current decays so that both EMIC losses and magneto-

pause losses are reduced, and the continuing action of ULF waves redistributes the remaining flux through radial diffusion [Shprits *et al.*, 2006b].

#### 4. Conclusions

[37] Using data from the HEO, SAMPEX, ACE, POES, and FAST satellites, the development of the relativistic electron flux dropout event which occurred on 20 November 2003 has been presented. Observations of the trapped energetic fluxes as a function of energy from HEO showed that the dropout event displayed different characteristics in different regions: at low  $L$ -shells ( $L < 5$ ) the electron depletion was strongly energy-dependent, increasing with increasing electron energy, and having a minimum energy cutoff near  $\sim 0.63$  MeV below which the depletion was no longer energy-dependent. At higher  $L$ -shells ( $L > 5$ ), all the energy channels were depleted to the same degree and did not exhibit an energy dependence.

[38] Coincident with the dropout, intense electron precipitation bands of energies  $> 1$  MeV were observed on the SAMPEX satellite when it was in the night sector, which moved from high  $L$ -shells ( $L \sim 6$ ) to low  $L$ -shells ( $L \sim 2$ ) during the development of the dropout event, following closely the estimated location of the plasmopause, and reaching a peak intensity during the main phase of the storm in the region  $2 < L < 5$ . Simultaneously, proton precipitation bands were observed on the POES satellite, which moved radially inward during the development of the dropout event, coincident with the electron precipitation bands, and reaching peak intensity in the same region. Owing to the orbit of the POES satellite, it was demonstrated that there was a large MLT asymmetry in the proton precipitation bands, occurring preferentially in the dusk sector. Using FAST data, it was shown that the proton precipitation bands occurred at a latitude of several degrees below the auroral region, thus excluding the possibility that scattering was due to local waves generated by auroral electrons, and that proton precipitation occurred preferentially on the duskside (confirming POES observations). In addition, the  $< 30$  keV electron channel showed that there were no precipitating electrons at these low energies, confirming the fact that the precipitation bands observed on SAMPEX only occurred at relativistic energies.

[39] Using these observations and results from previous studies, it is suggested that the dropout may be caused by two separate mechanisms acting respectively at high and low  $L$ -shells. At the high  $L$ -shells ( $L > 5$ ), losses to the magnetopause aided by the  $Dst$  effect and outward radial diffusion could deplete relativistic electrons down to  $L \sim 5$ . At low  $L$ -shells, strong diffusion driven by EMIC waves may result in a rapid loss of relativistic electrons, near the plasmopause and in plumes in the dusk sector. A sequence of events was proposed to explain the diffusion of energetic electrons from high pitch angles all the way to the loss cone, involving interaction with whistler mode chorus wave, plasmaspheric hiss, and EMIC waves at different parts of the drift orbit of the energetic electrons. Since we have only dealt with scattering by EMIC waves in this paper, experimental verification of the other components of our proposed sequence remains a topic for future work.

[40] In this work, data from a single dropout event was analyzed using multiple instruments and spacecraft, which may have shown the spatial separation of the two proposed mechanisms most clearly, due to its unusual intensity. Nonetheless, these results should be treated as preliminary and tested in a statistical way with a larger number of cases.

[41] **Acknowledgments.** J. Bortnik and R. M. Thorne would like to acknowledge support by NSF grant ATM 0402615 and NASA grant NNG04GN44G. T. P. O'Brien would like to acknowledge support by NSF grant ATM 0202107 and NASA grant NAG5-10972. This work was supported under The Aerospace Corporation's Independent Research and Development Program, The Aerospace Corporation MOIE program (via U.S. Air Force under contract FA8802-04-C-0001). Y. Y. Shprits would like to acknowledge support by the NSF grant ATM-0603191. The authors thank the SAMPEX science team for providing the data used in this study, James Weygand for the propagated ACE data covering 20–22 November 2003, and helpful discussion with Joe Mazur and Bern Blake.

[42] Zuyin Pu thanks the reviewers for their assistance in evaluating this paper.

#### References

- Albert, J. M. (2003), Evaluation of quasi-linear diffusion coefficients for EMIC waves in a multispecies plasma, *J. Geophys. Res.*, *108*(A6), 1249, doi:10.1029/2002JA009792.
- Albert, J. M. (2005), Evaluation of quasi-linear diffusion coefficients for whistler mode waves in a plasma with arbitrary density ratio, *J. Geophys. Res.*, *110*, A03218, doi:10.1029/2004JA010844.
- Baker, D. N., G. M. Mason, O. Figueroa, G. Colon, J. G. Watzin, and R. M. Aleman (1993), An overview of the Solar, Anomalous, and Magnetospheric Particle Explorer (SAMPEX) mission, *IEEE Trans. Geosci. Remote Sens.*, *31*(3), 531.
- Baker, D. N., J. B. Blake, L. B. Callis, J. R. Cummings, D. Hovestadt, S. Kanekal, B. Blecker, R. A. Mewaldt, and R. D. Zwickl (1994), Relativistic electron acceleration and decay timescales in the inner and outer radiation belts: SAMPEX, *Geophys. Res. Lett.*, *21*, 409.
- Blake, J. B., W. A. Kolasinski, R. W. Fillius, and E. G. Mullen (1992), Injection of electrons and protons with energies of tens of MeV into  $L < 3$  on 24 March 1991, *Geophys. Res. Lett.*, *19*, 821.
- Blake, J. B., M. D. Looper, D. N. Baker, R. Nakamura, B. Klecker, and D. Hovestadt (1996), New high temporal and spatial resolution measurements by SAMPEX of the precipitation of relativistic electrons, *Adv. Space Res.*, *18*, 171.
- Blake, J. B., D. N. Baker, N. Turner, K. W. Ogilvie, and R. P. Lepping (1997), Correlation of changes in the outer zone relativistic electron population with upstream solar wind and magnetic field measurements, *Geophys. Res. Lett.*, *24*, 927.
- Brautigam, D. H., and J. M. Albert (2000), Radial diffusion analysis of outer radiation belt electrons during the October 9, 1990 magnetic storm, *J. Geophys. Res.*, *105*, 291.
- Carlson, C. W., R. F. Pfaff, and J. G. Watzin (1998), The Fast Auroral Snapshot (FAST) mission, *Geophys. Res. Lett.*, *25*, 2012.
- Carlson, C. W., J. P. McFadden, P. Turin, D. W. Curtis, and A. Magoncelli (2001), The electron and ion plasma experiment for FAST, *Space Sci. Rev.*, *98*, 33.
- Cattell, C., L. Johnson, R. Bergmann, D. Klumpar, C. Carlson, J. McFadden, R. Strangeway, R. Ergun, K. Sigsbee, and R. Pfaff (2002), FAST observations of discrete electrostatic waves in associated with down-going ion beams in the auroral zone, *J. Geophys. Res.*, *107*(A9), 1238, doi:10.1029/2001JA000254.
- Cook, W. R., et al. (1993), PET: A Proton/electron telescope for studies of magnetospheric, solar, and galactic particles, *IEEE Trans. Geosci. Remote Sens.*, *31*, 565.
- Cornwall, J. M., F. V. Coroniti, and R. M. Thorne (1970), Turbulent loss of ring current protons, *J. Geophys. Res.*, *75*, 4699.
- Desorgher, L., P. Buhler, A. Zehnder, and E. O. Fluckiger (2000), Simulation of the outer radiation belt electron flux decrease during March 26, 1995, magnetic storm, *J. Geophys. Res.*, *105*, 21,211.
- Dessler, A. J., and R. Karplus (1961), Some effects of diamagnetic ring currents on Van Allen radiation, *J. Geophys. Res.*, *66*, 2289.
- Ebihara, Y., M.-C. Fok, S. Sazykin, M. F. Thomsen, M. R. Hairston, D. S. Evans, F. J. Rich, and M. Ejiri (2005), Ring current and the magnetosphere-ionosphere coupling during the superstorm of 20 November 2003, *J. Geophys. Res.*, *110*, A09S22, doi:10.1029/2004JA010924.
- Elphic, R. C., J. D. Means, R. C. Snare, R. J. Strangeway, L. Kepko, and R. E. Ergun (2001), Magnetic field instruments for the FAST Auroral Snapshot Explorer, *Space Sci. Rev.*, *98*, 151.

- Erlanson, R. E., and A. J. Ukhorskiy (2001), Observations of electromagnetic ion cyclotron waves during geomagnetic storms: wave occurrence and pitch angle scattering, *J. Geophys. Res.*, *106*, 3883.
- Evans, D. S., and M. S. Greer (2000), Polar-Orbiting Environmental Satellite Space Environment Monitor 2: Instrument description and archive data documentation, *Tech. Memo. OAR SEC-93*, NOAA, Boulder, Colo. (Available at <http://www.ngdc.noaa.gov/stp/NOAA/docs/SEM2v1.4b.pdf>)
- Foster, J. C., et al. (2005), Multiradar observations of the polar tongue of ionization, *J. Geophys. Res.*, *110*, A09S31, doi:10.1029/2004JA010928.
- Fraser, B. J., and T. S. Nguyen (2001), Is the plasmopause a preferred region of electromagnetic ion cyclotron waves in the magnetosphere?, *J. Atmos. Sol. Terr. Phys.*, *63*, 1225.
- Friedel, R. H. W., G. D. Reeves, and T. Obara (2002), Relativistic electron dynamics in the inner magnetosphere—a review, *J. Atmos. Sol. Terr. Phys.*, *64*, 265.
- Glauert, S. A., and R. B. Horne (2005), Calculation of pitch angle and energy diffusion coefficients with the PADIE code, *J. Geophys. Res.*, *110*, A04206, doi:10.1029/2004JA010851.
- Green, J. C., T. G. Onsager, T. P. O'Brien, and D. N. Baker (2004), Testing loss mechanisms capable of rapidly depleting relativistic electron flux in the Earth's outer radiation belt, *J. Geophys. Res.*, *109*, A12211, doi:10.1029/2004JA010579.
- Horne, R. B., and R. M. Thorne (1993), On the preferred source location for the convective amplification of ion cyclotron waves, *J. Geophys. Res.*, *98*, 9233.
- Horne, R. B., et al. (2005a), Wave acceleration of electrons in the Van Allen radiation belts, *Nature*, *437*, 227, doi: 10.1038/nature03939.
- Horne, R. B., R. M. Thorne, S. A. Glauert, J. M. Albert, N. P. Meredith, and R. R. Anderson (2005b), Timescale for radiation belt electron acceleration by whistler mode chorus waves, *J. Geophys. Res.*, *110*, A03225, doi:10.1029/2004JA010811.
- Jordanova, V. K., A. Boonsirisetth, R. M. Thorne, and Y. Dotan (2003), Ring current asymmetry from global simulations using a high-resolution electric field model, *J. Geophys. Res.*, *108*(A12), 1443, doi:10.1029/2003JA009993.
- Kennel, C. F., and F. Engelmann (1966), Velocity space diffusion from weak plasma turbulence in a magnetic field, *Phys. Fluids*, *9*, 2377.
- Kim, H.-J., and A. A. Chan (1997), Fully adiabatic changes in storm time relativistic electron fluxes, *J. Geophys. Res.*, *102*, 22,107.
- Koons, H. C., A. L. Vampola, and D. A. McPherson (1972), Strong pitch angle scattering of energetic electrons in the presence of electrostatic waves above the ionospheric trough region, *J. Geophys. Res.*, *77*, 1771.
- Li, X., I. Roth, M. Temerin, J. R. Wygant, M. K. Hudson, and J. B. Blake (1993), Simulation of the prompt energization and transport of radiation belt particles during the March 24, 1991 SSC, *Geophys. Res. Lett.*, *20*, 2423.
- Lorentzen, K. R., M. P. McCarthy, G. K. Parks, J. E. Foat, R. M. Millan, D. M. Smith, R. P. Lin, and J. P. Treilhou (2000), Precipitation of relativistic electrons by interaction with electromagnetic ion cyclotron waves, *J. Geophys. Res.*, *105*, 5381.
- Lorentzen, K. R., J. B. Blake, U. S. Inan, and J. Bortnik (2001), Observations of relativistic electron microbursts in association with VLF chorus, *J. Geophys. Res.*, *106*, 6017.
- Lyons, L. R., and R. M. Thorne (1972), Parasitic pitch angle diffusion of radiation belt particles by ion cyclotron waves, *J. Geophys. Res.*, *77*, 5608.
- Mathie, R. A., and I. R. Mann (2000), A correlation between extended intervals of ULF wave power and storm-time geosynchronous relativistic electron flux enhancements, *Geophys. Res. Lett.*, *27*, 3261.
- Meier, R. R., G. Crowley, D. J. Strickland, A. B. Christensen, L. J. Paxton, D. Morrison, and C. L. Hackert (2005), First look at the 20 November 2003 superstorm with TIMED/GUVI: Comparisons with a thermospheric global circulation model, *J. Geophys. Res.*, *110*, A09S41, doi:10.1029/2004JA010990.
- Meredith, N. P., R. B. Horne, and R. R. Anderson (2001), Substorm dependence of chorus amplitudes: Implications for the acceleration of electrons to relativistic energies, *J. Geophys. Res.*, *106*, 13,165.
- Meredith, N. P., R. M. Thorne, R. B. Horne, D. Summers, B. J. Fraser, and R. R. Anderson (2003), Statistical analysis of relativistic electron energies for cyclotron resonance with EMIC waves observed on CRRES, *J. Geophys. Res.*, *108*(A6), 1250, doi:10.1029/2002JA009700.
- Millan, R. M., R. P. Lin, D. M. Smith, K. R. Lorentzen, and M. P. McCarthy (2002), X-ray observations of MeV electron precipitation with a balloon-borne germanium spectrometer, *Geophys. Res. Lett.*, *29*(24), 2194, doi:10.1029/2002GL015922.
- Nagai, T. (1988), "Space weather forecast": Prediction of relativistic electron intensity at synchronous orbit, *Geophys. Res. Lett.*, *15*, 425.
- Nakamura, R., D. N. Baker, J. B. Blake, S. Kanekal, B. Klecker, and D. Hovestadt (1995), Relativistic electron precipitation enhancements near the outer edge of the radiation belt, *Geophys. Res. Lett.*, *22*, 1129.
- Nakamura, R., M. Isowa, Y. Kamide, D. N. Baker, J. B. Blake, and M. Looper (2000), SAMPEX observations of precipitation bursts in the outer radiation belt, *J. Geophys. Res.*, *105*, 15,875.
- O'Brien, T. P., and M. B. Moldwin (2003), Empirical plasmopause models from magnetic indices, *Geophys. Res. Lett.*, *30*(4), 1152, doi:10.1029/2002GL016007.
- O'Brien, T. P., M. D. Looper, and J. B. Blake (2004), Quantification of relativistic electron microburst losses during the GEM storms, *Geophys. Res. Lett.*, *31*, L04802, doi:10.1029/2003GL018621.
- O'Brien, T. P., J. C. Green, J. E. Mazur, and M. D. Looper (2005), Electron precipitation bands: possible causes, expectations, and observations, *Eos Trans. AGU*, *86*(18), Jt. Assem. Suppl., Abstract SM23C-01.
- Onsager, T. G., G. Rostoker, H.-J. Kim, G. D. Reeves, T. Obara, H. J. Singer, and C. Smithro (2002), Radiation belt electron flux dropouts: local time, radial and particle-energy dependence, *J. Geophys. Res.*, *107*(A11), 1382, doi:10.1029/2001JA000187.
- Reeves, G. D., K. L. McAdams, R. H. W. Friedel, and T. P. O'Brien (2003), Acceleration and loss of relativistic electrons during geomagnetic storms, *Geophys. Res. Lett.*, *30*(10), 1529, doi:10.1029/2002GL016513.
- Roederer, J. G. (1970), *Dynamics of Geomagnetically Trapped Radiation*, Springer, New York.
- Selesnick, R. S., and J. B. Blake (1997), Dynamics of the outer radiation belt, *Geophys. Res. Lett.*, *24*, 1347.
- Selesnick, R. S., and J. B. Blake (2000), On the source location of radiation belt relativistic electrons, *J. Geophys. Res.*, *105*, 2607.
- Shprits, Y. Y., R. M. Thorne, R. B. Horne, S. A. Glauert, M. Cartwright, C. T. Russell, D. N. Baker, and S. G. Kanekal (2006a), Acceleration mechanism responsible for the formation of the new radiation belt during the 2003 Halloween solar storm, *Geophys. Res. Lett.*, *33*, L05104, doi:10.1029/2005GL024256.
- Shprits, Y. Y., R. M. Thorne, R. Friedel, G. D. Reeves, J. F. Fennell, D. Baker, and S. G. Kanekal (2006b), Outward radial diffusion driven by losses at magnetopause, *J. Geophys. Res.*, *111*, A11214, doi:10.1029/2006JA011657.
- Shprits, Y. Y., W. Li, and R. M. Thorne (2006c), The controlling effects of the pitch angle scattering rates near the edge of the loss cone on electron lifetimes, *J. Geophys. Res.*, doi:10.1029/2006JA011758, in press.
- Shue, J.-H., P. Song, C. T. Russell, J. T. Steinberg, J. K. Chao, G. Zastenker, O. L. Vaisberg, S. Kokubun, H. J. Singer, T. R. Detman, and H. Kawano (1998), Magnetopause location under extreme solar wind conditions, *Geophys. Res. Lett.*, *103*, 17,691.
- Spasojevic, M., M. F. Thomsen, P. J. Chi, and B. R. Sandel (2005), Afternoon subauroral proton precipitation resulting from ring current-plasmasphere interaction, in *Inner Magnetosphere Interactions: New Perspectives from Imaging*, *Geophys. Monogr. Ser.*, volume 159, edited by J. L. Burch, M. Schulz, and H. Spence, pp. 85–100, AGU, Washington, D. C.
- Stern, D. P. (1996), A brief history of magnetospheric physics during the space age, *Rev. Geophys.*, *34*, 1.
- Stone, E. C., A. M. Frandsen, R. A. Mewaldt, E. R. Christian, D. Margolies, J. Ormes, and F. Snow (1998), The Advanced Composition Explorer, *Space Sci. Rev.*, *86*, 1.
- Summers, D., and R. M. Thorne (2003), Relativistic electron pitch angle scattering by electromagnetic ion cyclotron waves during geomagnetic storms, *J. Geophys. Res.*, *108*(A4), 1143, doi:10.1029/2002JA009489.
- Thorne, R. M., and C. F. Kennel (1971), Relativistic electron precipitation during magnetic storm main phase, *J. Geophys. Res.*, *76*, 4446.
- Thorne, R. M., T. P. O'Brien, Y. Y. Shprits, D. Summers, and R. B. Horne (2005), Timescale for MeV electron microburst loss during geomagnetic storms, *J. Geophys. Res.*, *110*, A09202, doi:10.1029/2004JA010882.
- Thorne, R. M., R. B. Horne, V. K. Jordanova, J. Bortnik, and S. Glauert (2006), Interaction of EMIC waves with thermal plasma and radiation belt particles, in *Magnetospheric ULF Waves*, *Geophys. Monogr. Ser.*, edited by K. Takahashi, B. Lysak, and P. Chi, AGU, Washington, D. C., in press.
- Vampola, A. L. (1977), The effect of strong pitch angle scattering on the location of the outer-zone electron boundary as observed by low-altitude satellites, *J. Geophys. Res.*, *82*, 2289.
- Walt, M., and H. D. Voss (2004), Proton precipitation during magnetic storms in August through November 1998, *J. Geophys. Res.*, *109*, A02201, doi:10.1029/2003JA010083.
- Weimer, D. R., D. M. Ober, N. C. Maynard, M. R. Collier, D. J. McComas, N. F. Ness, C. W. Smith, and J. Watermann (2003), Predicting interplanetary magnetic field (IMF) propagation delay times using the minimum variance technique, *J. Geophys. Res.*, *108*(A1), 1026, doi:10.1029/2002JA009405.
- West, H. I., Jr., R. M. Buck, and J. R. Walton (1972), Observation of the shadowing of electron azimuthal-drift motions near the noon magnetopause, *Nature*, *240*, 6.

Yizengaw, E., M. B. Moldwin, A. Komjathy, and A. J. Manucci (2006), Unusual topside ionospheric density response to the November 2003 superstorm, *J. Geophys. Res.*, *111*, A02308, doi:10.1029/2005JA011433.

---

D. N. Baker, Laboratory for Atmospheric and Space Physics, University of Colorado, Campus Box 590, Boulder, CO 80309, USA. (daniel.baker@lasp.colorado.edu)

J. Bortnik, Y. Y. Shprits, and R. M. Thorne, Department of Atmospheric and Oceanic Sciences, University of California, Los Angeles, Math

Sciences Building, Los Angeles, CA 90095-1565, USA. (jbortnik@gmail.com; yshprits@atmos.ucla.edu; rmt@atmos.ucla.edu)

J. C. Green, NOAA, 325 Broadway, Boulder, CO 80303-3328, USA. (janet.green@noaa.gov)

T. P. O'Brien, Space Sciences Department/Chantilly, The Aerospace Corporation, 15049 Conference Center Drive, CH3/210, Chantilly, VA 20151-3824, USA. (paul.obrien@aero.org)

R. J. Strangeway, Institute of Geophysics and Planetary Physics, University of California, Los Angeles, Los Angeles, CA 90024-1567, USA. (strange@igpp.ucla.edu)